Available online at www.sciencedirect.com

ScienceDirect

J Materiomics 1 (2015) 333–339

www.ceramsoc.com/en/

www.journals.elsevier.com/journal-of-materiomics/

Synthesis of sulfur encapsulated 3D graphene sponge driven by micro-pump and its application in Li–S battery

Qin Zhang, Shuangjie Tan, Xin Kong, Yao Xiao, Lei Fu*

College of Chemistry and Molecular Science, Wuhan University, Wuhan 430072, China

Received 27 May 2015; revised 14 October 2015; accepted 23 October 2015
Available online 3 November 2015

Abstract

Because of advantages such as excellent conductivity and high theoretical specific surface area, 3D graphene sponge (3D-GS) grown on Ni template via chemical vapor deposition (CVD) is receiving increasing attention as a conducting template to improve the conductivity of electrode in lithium sulfur (Li–S) battery. However, loading sulfur on the surface of 3D-GS is not a feasible approach to remit the dissolution of polysulfides in cathodes or improve the cycling of batteries. Here, we report a novel design inspired from micro-pump and synthesize a sulfur encapsulated 3D graphene sponge (3D-GS@S) material for Li–S battery for the first time. Under the oil–water two phase liquid seal system, consisting of sulfur-containing organic phase and etching water phase, the vacuum cavities would generate from Ni etching. Tactfully, the pressure differences between vacuum cavities and sulfur-containing solution were converted into driving force for pumping the sulfur-containing solution into 3D-GS. As a result, the sulfur particles uniformly anchored on the inner surface of 3D-GS after the volatilization of sulfur-containing solution. Serving 3D-GS@S as cathode material does not require any additional conducting additives, current collector or binders thus increasing the loading contents of sulfur. A Li–S battery with 3D-GS@S material cathode shows good electrochemical stability and high rate discharge capacity retention for up to 160 discharge/charge cycles at a high rate of 1C. Our results demonstrate the promising suitability of 3D-GS@S for efficient and high performance rechargeable Li–S batteries.

Keywords: Li–S battery; 3D graphene sponge; Sulfur cathode; Micro-pump; High-rate stability

1. Introduction

Lithium sulfur batteries, with unparalleled theoretical capacity (1675 mAh/g), ultrahigh energy density (~2600 Wh/kg) and other advantages, have drawn tremendous attentions owing to their great potential for applications in next-generation clean and efficient high energy power system [1–3]. Next to oxygen, elemental sulfur is an intriguing cathode material which is also low cost, abundant, and nontoxic [4–6]. Despite the appealing theoretical characteristics, the practical applications of Li–S batteries are mainly restricted by the poor electrochemical performance of sulfur. Furthermore, unlike batteries with intercalation compounds, Li–S batteries experience the dissolution and diffusion of reaction intermediates (lithium polysulfides, Li_2S_x, $2 < x \leqq 8$) into the electrolyte. These two major challenges can lead to a loss of active materials from the cathode and to a polysulfide shuttle effect, resulting in capacity fading and poor coulombic efficiency [7,8]. To alleviate these issues, several scientific and technological innovations have been proposed, such as forming a protective film on the lithium anode [9,10], ameliorative electrolyte [11,12], modified separator [13,14], and fabricating composite electrodes of sulfur/polymer [15–18], sulfur/metal organic framework (MOF) [19] and sulfur/carbon [20–23].

3D graphene sponge (3D-GS) with excellent electrical conductivity and 3D interconnected structure is emerging as one of the most promising conducting template for lithium ion

* Corresponding author. Tel.: +86 027 6875 5867.
E-mail address: leifu@whu.edu.cn (L. Fu).
Peer review under responsibility of The Chinese Ceramic Society.

http://dx.doi.org/10.1016/j.jmat.2015.10.002

battery [24–27]. The synergistic effect of conductivity and network structure facilitates rapid electron and ion transport. Recently, binder-free 3D-GS/sulfur composite (3D-GS@S) has been reported as a cathode in Li–S battery system, which demonstrates a great potential of using 3D-GS to load sulfur as a novel cathode structure [28]. For the sake of remitting the dissolution and diffusion of reaction intermediates in Li–S battery, encapsulating sulfur in the 3D-GS shows more effective when compared with sulfur loading on the surface of 3D-GS. As a result, it is important to obtain sulfur well coated and confined by 3D-GS. Nonetheless, encapsulating sulfur in the 3D-GS, until now, has not been reported.

In this work, we present a novel design inspired from micro-pump and synthesis of sulfur encapsulated 3D-GS (3D-GS@S) composite as a Li–S battery cathode for the first time. In brief, the 3D-GS is synthesized via CVD from a nickel catalyst template. Ni, making bare contribution to the discharge/charge capacity of Li–S battery, should be etched away generally. Herein, we deposited the 3D-GS with Ni template on the interface between sulfur/n-pentane solution (oil phase) and $FeCl_3$ solution (water phase). We utilized Ni etching to generate vacuum cavities, to form pressure differences naturally, so as to suck the sulfur-containing solution into 3D-GS. This approach succeeds in realizing Ni etching and active sulfur loading at the same time, and constituting the expectant structure of encapsulating sulfur in the 3D-GS. On the premise of keeping the outstanding conductivity and high specific surface area of 3D-GS, we applied the 3D-GS@S material to Li–S battery cathode. Furthermore, departing from the normal practice in conventional Li–S batteries, we have been able to eliminate any additional metal current collectors, conducting additives and binders. The 3D-GS@S cathode material showed excellent high-rate stability and decent columbic efficiency over 160 cycles in a Li–S battery.

2. Experimental section

2.1. The growth of 3D-GS

The 3D-GS was synthesized by CVD via Ni foam template from CH_4 and H_2 at atmospheric pressure in a quartz tube furnace at 1000 °C. The growth process consisted of four steps: (1) the nickel foam was heated to 1000 °C in 30 min under the atmosphere of Ar (500 sccm) and H_2 (50 sccm), then annealed at 1000 °C for 10 min without changing the gas flow; (2) a nominal amount of CH_4 (5 sccm) was brought into the reaction tube at ambient pressure for 5 min; (3) the samples were cooled to room temperature naturally with Ar (500 sccm). After the CVD growth process, Ni foam covered with 3D-GS was slowly drop-coated by PMMA/acetone solution (1:1 in volume), which was then placed on a hotplate and heated to 110 °C. After the solution was dried off, another drop was added. This process was repeated several times until a desired PMMA loading was obtained. Then the Ni/graphene sponge/PMMA composite was held at that temperature for 1 h.

2.2. The preparation of sulfur/n-pentane solution

2.7 g Na_2S was dissolved in 50 mL of ultrapure water to form a Na_2S solution, then 0.9 g $Na_2S_2O_3 \cdot 5H_2O$ was added into the solution with magnetic stirring. 10 mL 2 M formic acid (HCOOH) was instilled into the as-obtained aqueous solution and stirred for another 0.5 h. The reaction can be expressed as: $Na_2S_2O_3 + 2Na_2S + 6HCOOH = 6HCOONa + 3H_2O + 4S\downarrow$. 50 mL n-pentane was added to the as-prepared solution after it was cooled to room temperature. Then the mixture was transferred to a separating funnel and fiercely oscillated. After liquid–solid extraction, the sulfur/n-pentane solution was obtained.

2.3. The synthesis of 3D-GS@S composite

The sulfur/n-pentane solution was added into a beaker which was contained with 1 M $FeCl_3$ solution. The Ni/graphene sponge/PMMA composite was placed between oil–water two-phase to ensure Ni etching and sulfur loading simultaneously. After one whole night, the sulfur/graphene sponge/PMMA composite was washed with 1 M HCl and ultrapure water for several times to remove salts and impurities. Subsequently, in order to remove the PMMA, the parched product was washed three times with acetone and finally dried in vacuum at 60 °C for 12 h.

2.4. Characterization

Raman spectroscopy was measured with a laser micro-Raman spectrometer (Renishaw in Via, Renishaw, 532 nm excitation wavelength). Scanning electron microscopy (SEM) was performed in a ZEISS Merlin Compact SEM and energy dispersive X-ray spectroscopy (EDX) was collected using an INCAPentalFETx3 Oxford EDX. Transmission Electron Microscopy (TEM) was performed using a JEM-2100 (JEOL Ltd., Japan). X-Ray diffraction measurement was performed with LabX XRD-6000 using Cu-Kα radiation over the range of $2\theta = 10°–80°$. Thermogravimetric analysis (TGA) was conducted under ambient pressure on a TGA Q500 (Thermal Analysis Instrument, Burlington) in nitrogen with a heating rate of 10 °C/min from room temperature to 600 °C.

2.5. Electrochemical measurements

The electrochemical performances of the composites were evaluated by using standard CR2016 coin-type cells with a lithium metal anode. The cells were assembled in an Ar-filled glovebox by directly using the as-prepared interconnected graphene as working electrode without adding any binder or conductive agents and lithium metal circular foil (1.5 mm) as counter electrode. 1.0 M $LiN(CF_3SO_2)_2$ (1 M) (99.95%, trace metals basis, Sigma–Aldrich) salt dissolved in a mixture of dioxolane (DOL) (99.8%, Sigma–Aldrich) and 1,2-dimethoxyethane (DME) (99.5, Sigma–Aldrich) in a volume ratio of 1:1 containing $LiNO_3$ (1 wt%) was used as the electrolyte. Galvanostatical charge–discharge tests were conducted at

various current densities at the voltage range from 1.00 V to 3.00 V with a multichannel battery tester (LAND CT 2001A, Wuhan LAND Electronics CO., Ltd). The cyclic voltammetry (CV) tests were measured using electrochemical workstation (CHI610E, Chenhua, Shanghai) at a sweeping rate of 0.2 mV s^{-1} with the voltage ranging from 1.50 V to 3.00 V. Electrochemical impedance spectroscopy (EIS) tests were measured in the frequency range from 100 kHz to 0.1 Hz on a electrochemical workstation (Im6e, Zahner).

3. Results and discussion

In our approach, as shown in Fig. 1a, the PMMA-protected 3D-GS was deposited on the interface between oil phase (sulfur/n-pentane solution) and water phase (1 M $FeCl_3$ solution). Sulfur particles were well dispersed in the oil phase, while Ni was etched by the $FeCl_3$ solution. Graphene is inclined to be intercalated and to form micro-pores in the defects on account of the $FeCl_3$ etching [29]. Due to the Ni etching and the dissolution of $NiCl_2$, many vacuum cavities would be generated which were subsequently served as capillaries. In the combination of etching and the pressure of upper solution, the vacuum cavities may grow into larger bubbles (Fig. 1a). As a result of the liquid seal, the difference in pressure between the vacuum cavities and upper solution would generate. Under the pressure differences, the sulfur/n-pentane solution was automatically sucked into the graphene sponge. Fig. 1b reveals the existence of pores resulting from etching and the pore size was mainly distributed between 1 ~2 μm (Fig. 1c).

Fig. 1d shows a schematic overview of the etching process and sulfur loading, involved in the synthesis of 3D-GS@S composite. According to the capillary phenomenon, the rising height of the solution can be expressed as:

$$h = \frac{2\gamma}{R\rho_l g} \quad (1)$$

wherein γ and ρ_l respectively represent the surface tension and density of injected solution. R stands for the diameter of capillary. Taking n-pentane for example, when sets the value of R as 2 μm, the calculated rising height is about 2.53 mm. In comparison with the ~100 μm width of graphene framework, the rising height would meet the requirement of filling the graphene sponge. It is worth to note that the surface of graphene is hydrophobic which also contributes to the sucking force to some extent. Then the constantly formed bubbles and vacuum cavities might act as numerous micro-pumps, sucking the sulfur/n-pentane solution into 3D-GS continuously until the pressure differences disappeared. After the volatilization of n-pentane solution, sulfur preserved and anchored on the inner surface of graphene sponge, in-situ replacing the original Ni foam with sulfur. Moreover, the loading sulfur contents can be well controlled by adjusting the concentration of sulfur/n-pentane solution. Since the PMMA were removed, with 3D network structure retained, the 3D-GS@S composite was eventually obtained. Above all, the composite structure of sulfur encapsulated graphene not only takes full advantages of graphene who shows superiority in conductivity and specific surface area, but also effectively remits the volume expansion during discharge of active materials.

Fig. 2a is the Raman spectra of 3D-GS@S composite and 3D-GS, which shows distinct 2D-band (~2700 cm^{-1}) and G-band (~1580 cm^{-1}) peaks with a I_G/I_{2D} ratio >1, indicating the formation of multilayered graphene sponge [30]. As the D-band (~1350 cm^{-1}) is attributable to disordered carbon and indicative of the extent defects of graphene, there is no observable D peak, indicative of the high crystalline quality [30]. Moreover, the indiscernible D-band of 3D-GS@S composite indicates that only few defects were introduced to the 3D-GS during the etching process. To investigate the crystallographic phase of sulfur, X-ray diffraction (XRD) patterns of the elemental sulfur and 3D-GS@S composite were performed (Fig. 2b). Usually, sulfur exists in a crystalline state with an

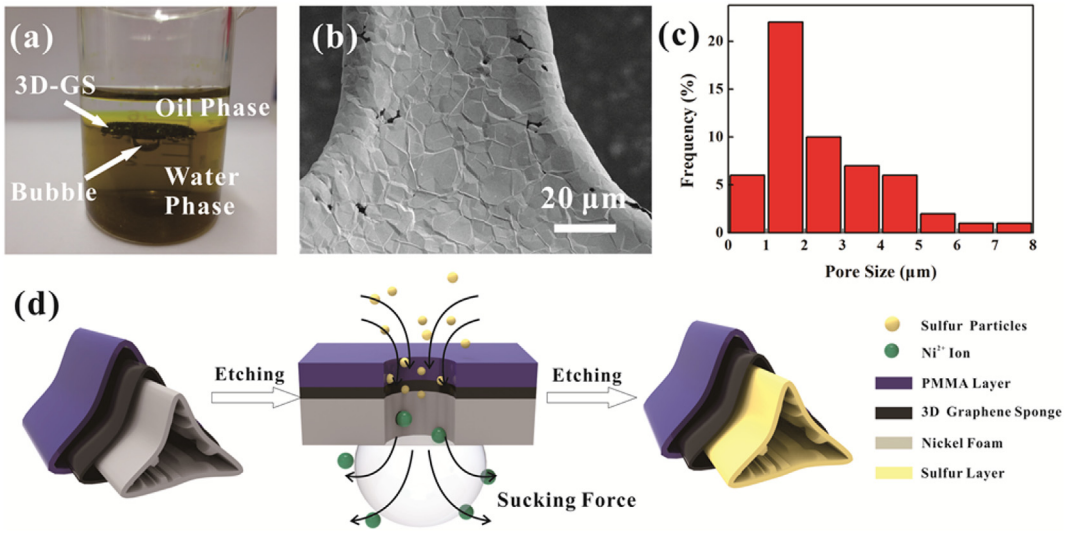

Fig. 1. (a) Digital camera image of the reaction process; (b, c) SEM image of the pores on graphene sponge and their pore size distribution; (d) a schematic overview of the etching and sulfur loading process involved in the synthesis of 3D-GS@S composite.

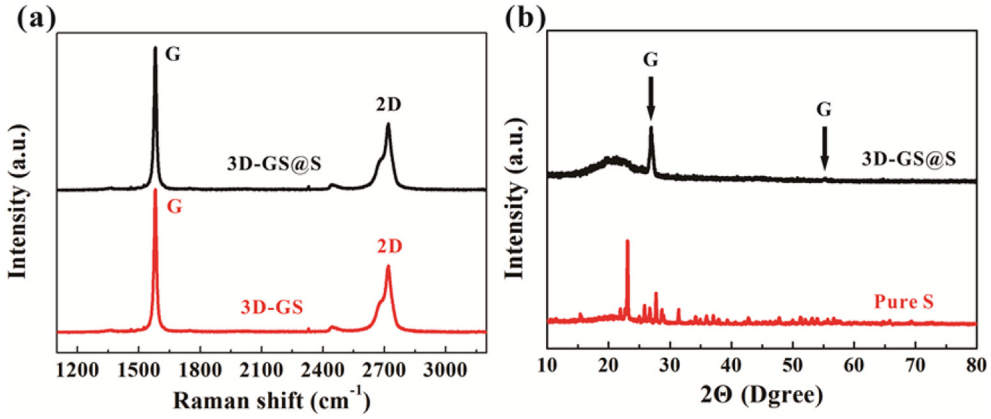

Fig. 2. (a) Raman spectra of 3D-GS@S and 3D-GS, (b) XRD patterns for 3D-GS@S and pure sulfur.

orthorhombic structure at room temperature. While sharp diffraction peaks are seen for pure sulfur, the peaks disappeared after impregnation into the 3D-GS, demonstrating that the sulfur existed in a highly dispersed amorphous state [31].

Fig. 3a–c show the scanning electron microscopy (SEM) images of the as-prepared 3D-GS@S composite after PMMA removal. To further confirm whether the sulfur was encapsulated by 3D-GS, the composite was cut in half to ensure applicable cross-section for SEM. As shown in Fig. 3a, the 3D-GS has an integrated 3D macro-porous structure which provides a stable reservoir for the electrolyte. The higher magnification SEM image of cross-section shows the hollow structure of 3D-GS, holding space for the expansion of sulfur. In order to confirm whether the sulfur was impregnated into the 3D-GS, the higher magnification SEM images near the cross-section were collected in Fig. 3b and c. Fig. 3b shows the ripples and wrinkles of the outer surface in 3D-GS without PMMA residue, while Fig. 3c shows the inner surface. The distinct morphology of two images indicates that the sulfur was well dispersed and anchored on graphene which is further corroborated by EDX. An elemental mapping for carbon (Fig. 3e) and sulfur (Fig. 3f) corresponding to the white square marked in the SEM image (Fig. 3d) indicates a uniform distribution of sulfur across the inner surface of 3D-GS. A very similar intensity distribution of carbon and sulfur could be

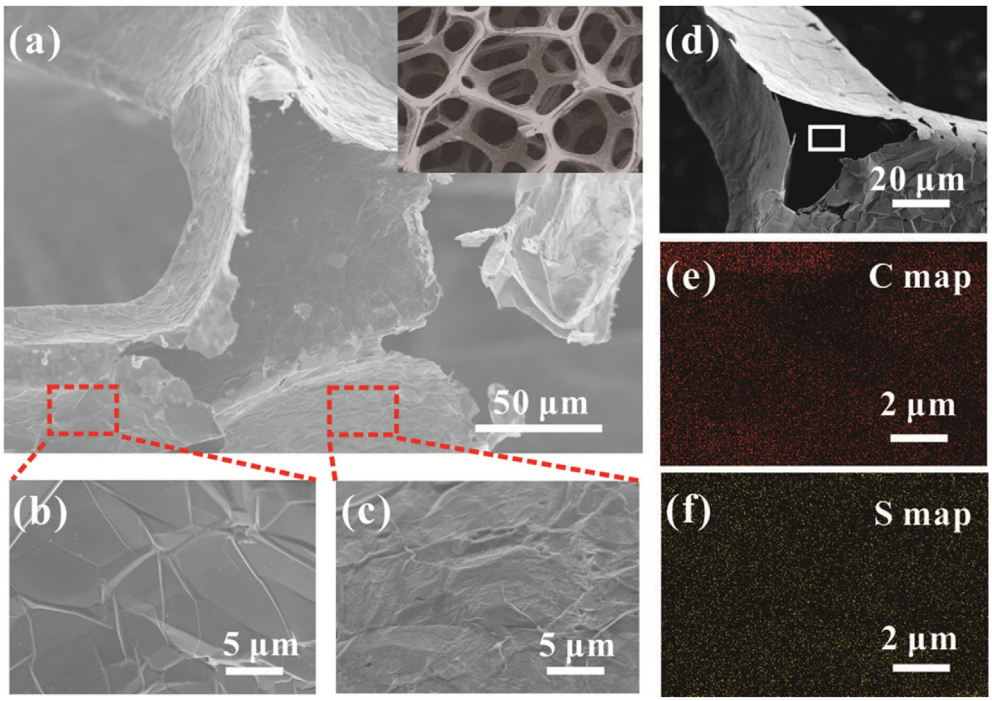

Fig. 3. (a–c) SEM images of 3D-GS@S composite in different magnifications, while (b) and (c) respectively correspond to the region shown in the two red squares; (d) SEM image of higher magnification; (e, f) EDX elemental mapping of (e) carbon and (f) sulfur correspond the region of white square shown in (d).

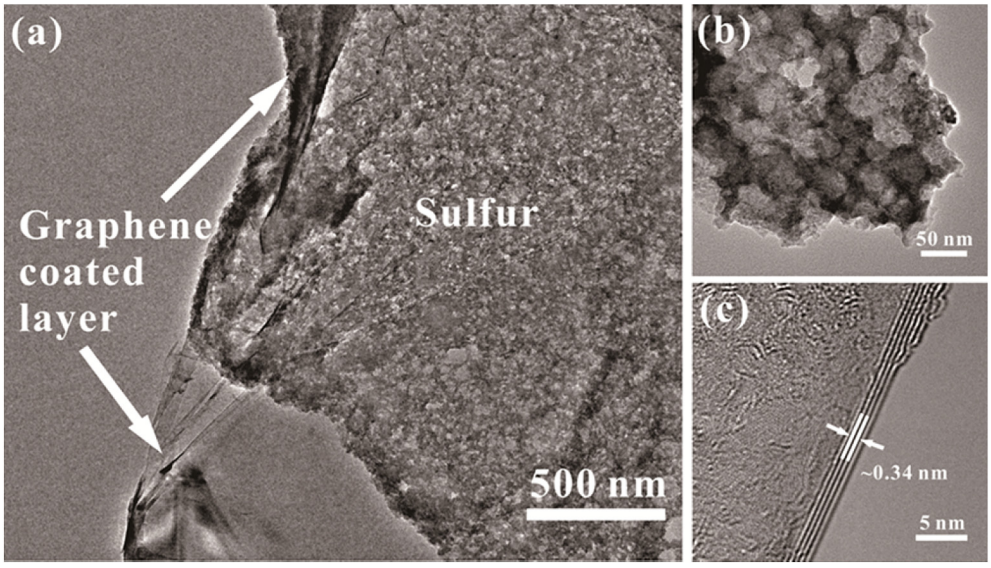

Fig. 4. TEM images of 3D-GS@S composite at low (a) and high (b) magnifications; (c) High-resolution TEM images of the 3D-GS cross section.

observed in the elemental mappings, preventing from block the electric conductivity of 3D-GS@S composite.

In order to further characterize 3D-GS@S composite in details, the transmission electron microscopy (TEM) images were characterized. Low magnification TEM image (Fig. 4a) shows a continuous film, which could be graphene sheet with sulfur attached to, was further characterized at higher magnifications (Fig. 4b, c). It is worth noting that even after fierce ultrasonication to disperse samples for TEM characterization, sulfur were still anchored to the surface of graphene, suggesting a strong interaction between graphene and sulfur in the combination of TGA. As shown in Fig. 4a, the light region was corresponding to the graphene coated layer, while the dark region was sulfur. Additionally, sulfur particles existing as uniformly dispersed were observed in the magnified TEM image (Fig. 4b). The high resolution cross-sectional TEM image (Fig. 4c) clearly shows ~4 graphene layers on top of each other with an adjacent fringe spacing of ~0.34 nm.

The sulfur contents of 3D-GS@S composite were measured by TGA under N_2 atmosphere, as shown in Fig. 5a. The sulfur particles anchored on 3D-GS was thermally stable and its weight loss happened at the range of 150–250 °C. And the weight loss in this analysis shows the appropriate ~66 wt% sulfur loading contents. The 3D-GS@S composite was incorporated as a cathode in a Li–S battery and Fig. 5b shows initial discharge/charge curves for cells at different C rates (C rate was based on the theoretical specific capacity of sulfur, where a 1C rate corresponded to a current density of 1675 mA/g). The discharge curves exhibited multiple stages corresponding to sequential reduction from S to Li_2S, while the charge process due to oxidation appeared relatively simple [32,33]. Cycling voltammetry was conducted and the result was shown in Fig. 5c. There were three distinguishable peaks in the cyclic scan. Two peaks were in the cathodic scans between 1.9 V and 2.4 V and a single peak at ~2.6 V in the reverse scans, which corresponds to the reduction and oxidation of sulfur, respectively. As shown in Fig. 5d, the EIS spectra were composed of a depressed semicircle in the high-frequency region and a sloping straight line in the low-frequency region. With the combination of 3D-GS, the overall electrical conductivity was enhanced. Cycling performance of the Li–S battery with 61% sulfur loading is considered in further details in Fig. 5e. After the initial capacity loss, the composite shows very high capacity retention upon cycling. At a rate of 1C, an initial capacity of 1010 mAh/g was measured and the specific capacity stays above ~500 mA/g after 160 cycles, representing good cycle stability. The average coulombic efficiency is computed to be ~80%, indicating decent stability. As expected, a Li–S battery with 3D-GS@S material cathode shows excellent high-rate stability and decent columbic efficiency, demonstrating its potential for electrode material of high performance batteries.

4. Conclusions

In summary, we have developed a one-step loading method to acquire sulfur encapsulated graphene composite structure, basing on the micro-pump and the conspicuous capillary phenomenon in our daily life. The 3D graphene sponge we synthesized could serve as conducting substrate and current collector, without any other conducting additives and binders. Furthermore, the graphene encapsulated layer effectively remits the dissolution of polysulfides, and accommodates some of the stress and volume expansion during discharge of sulfur. The 3D-GS@S electrode composite exhibits excellent high-rate discharge stability as cathode in a Li–S battery. At a rate of 1C, an initial capacity of 1010 mAh/g was measured and the specific capacity stays above ~500 mA/g after 160 cycles, representing good cycle stability. In the future, the one-step loading method will be of significant interest to further

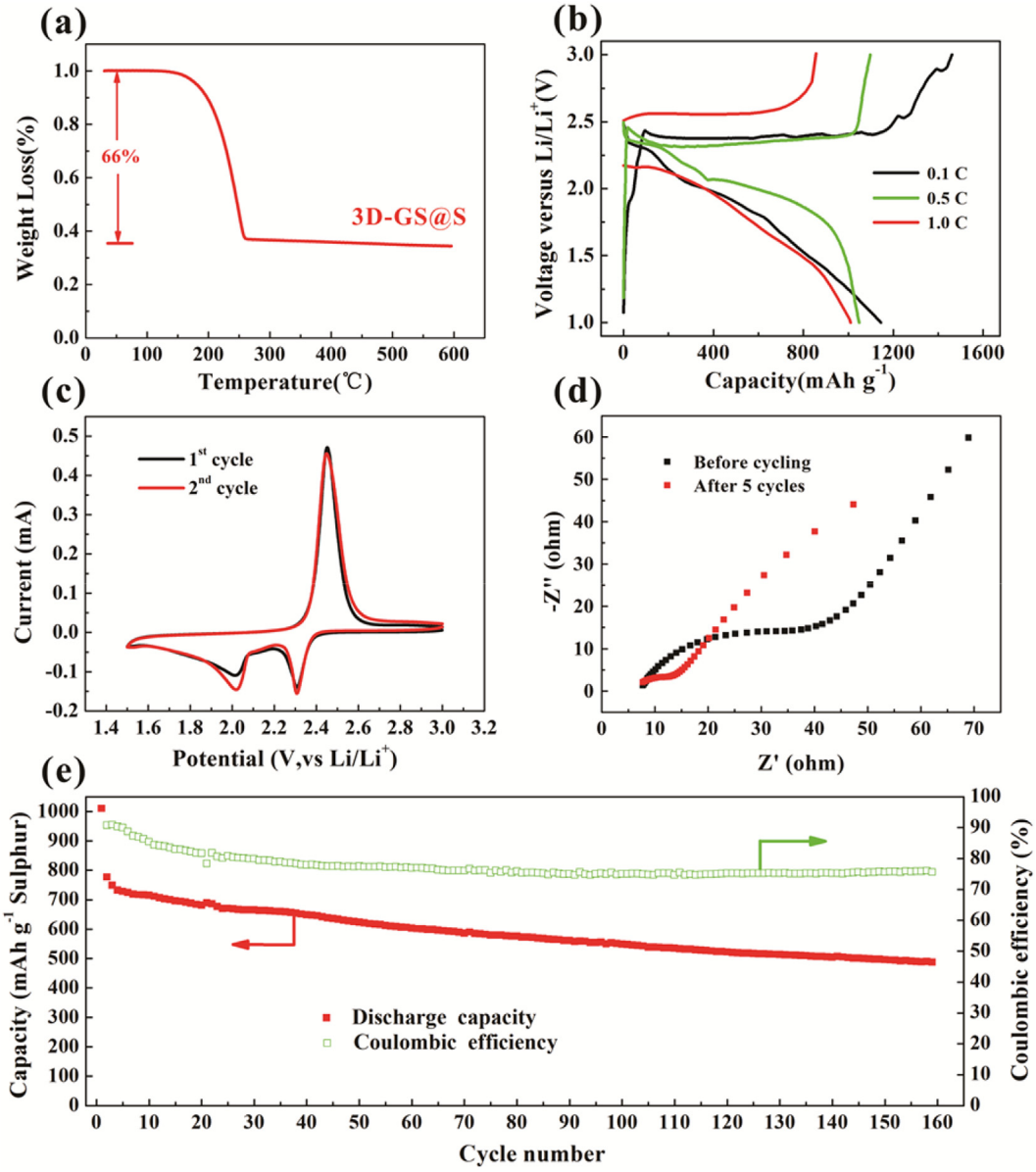

Fig. 5. (a) TGA curve of 3D-GS@S material; (b) Initial cycle charge and discharge voltage profiles at various rates; (c) CV curves of 3D-GS@S at a scan rate of 0.2 mV s^{-1} within a potential range of 1.5–3.0 V; (d) EIS spectra of 3D-GS@S fresh electrodes at open-circuit potential and after cycling for 5 cycles; (e) Cycle performance of sample at 1C.

stabilize the composite materials and applied to other electrode materials for high energy density rechargeable batteries.

Acknowledgments

The research was supported by the National Natural Science Foundation of China (Grants 51322209, 21473124), the Sino-German Center for Research Promotion (Grants GZ 871) and the Ministry of Education of the People's Republic of China (Grants 20120141110030). We thank Prof. Xinping Ai for the assembly of coin-type cells and Prof. Lin Zhuang who assists in the XRD and TGA characterizations. In addition, we also thank Prof. Mark H. Rümmeli and his student for TEM characterizations.

References

[1] Sun L, Kong WB, Jiang Y, Wu HC, Jiang KL, Wang JP, et al. Super-aligned carbon nanotube/graphene hybrid materials as a framework for sulfur cathodes in high performance lithium sulfur batteries. J Mater Chem A 2015;3:5305–12.

[2] Yin YX, Xin S, Guo YG, Wan LJ. Lithium–sulfur batteries: electrochemistry, materials and prospects. Angew Chem Int Ed 2013;52:13186–200.

[3] Yang J, Wang SY, Ma ZP, Du ZL, Li CY, Song JJ, et al. Novel nitrogen-doped hierarchically porous coralloid carbon materials as host matrixes for lithium–sulfur batteries. Electrochim Acta 2015;159:8–15.

[4] Ji LW, Rao MM, Zheng HM, Zhang L, Li YC, Duan WH, et al. Graphene oxide as a sulfur immobilizer in high performance lithium/sulfur cells. J Am Chem Soc 2011;133:18522–5.

[5] Ji X, Lee KT, Nazar LF. A highly ordered nanostructured carbon-sulphur cathode for lithium–sulphur batteries. Nat Mater 2009;8:500–6.

[6] Hassoun J, Scrosati B. A high-performance polymer tin sulfur lithium ion battery. Angew Chem 2010;122:2421–4.
[7] Song JX, Gordin ML, Xu T, Chen SR, Yu ZX, Sohn H. Strong lithium polysulfide chemisorption on electroactive sites of nitrogen-doped carbon composites for high-performance lithium–sulfur battery cathodes. Angew Chem Int Ed 2015;54:4325–9.
[8] Yang X, Zhang L, Zhang F, Huang Y, Chen YS. Sulfur-infiltrated graphene-based layered porous carbon cathodes for high-performance lithium–sulfur batteries. ACS Nano 2014;8:5208–15.
[9] Min Y, Soon N, Hwa J, Ki J. Electrochemical performance of lithium/sulfur batteries with protected li anodes. J Power Sources 2003;119–121:964–72.
[10] Wang QS, Jin J, Wu XW, Ma GQ, Yang JH, Wen ZY. A shuttle effect free lithium sulfur battery based on a hybrid electrolyte. Phys Chem Chem Phys 2014;16:21225–9.
[11] Aurbach D, Pollak E, Elazari R, Salitra G, Kelley CS, Affinito J. On the surface chemical aspects of very high energy density, rechargeable Li–sulfur batteries. J Electrochem Soc 2009;156:A694–702.
[12] Liang X, Wen ZY, Liu Y, Wu MF, Jin J, Zhang H, et al. Improved cycling performances of lithium sulfur batteries with Li_nO_3-modified electrolyte. J Power Sources 2011;196:9839–43.
[13] Zhou GM, Li L, Wang DW, Shan XY, Pei SF, Li F, et al. A flexible sulfur-graphene-polypropylene separator integrated electrode for advanced Li–S batteries. Adv Mater 2015;27:641–7.
[14] Ma GQ, Wen ZY, Wu MF, Shen C, Wang QS, Jin J, et al. A lithium anode protection guided highly-stable lithium–sulfur battery. Chem Commun 2014;50:14209–12.
[15] Wang JL, Yang J, Xie JY, Xu NX. A novel conductive polymer-sulfur composite cathode material for rechargeable lithium batteries. Adv Mater 2002;14:963–5.
[16] Zhao XH, Kima JK, Ahnb HJ, Chob KK, Ahna JH. A ternary sulfur/polyaniline/carbon composite as cathode material for lithium sulfur batteries. Electrochim Acta 2013;109:145–52.
[17] Ma GQ, Wen ZY, Jin J, Lu Y, Wu XW, Cai Liu, et al. Enhancement of long stability of Li–S battery by thin wall hollow spherical structured polypyrrole based sulfur cathode. RSC Adv 2014;4:21612–8.
[18] Ma GQ, Wen ZY, Jin J, Lu Y, Wu XW, Wu MF, et al. Hollow polyaniline sphere@sulfur composites for prolonged cycling stability of lithium–sulfur batteries. J Mater Chem A 2014;2:10350–4.
[19] Xi K, Cao S, Peng X, Ducati C, Kumar RV, Cheetham AK. Carbon with hierarchical pores from carbonized metal-organic frameworks for lithium sulphur batteries. Chem Commun 2013;49:2192–4.
[20] He G, Mandlmeier B, Schuster J, Nazar LF, Bein T. Bimodal mesoporous carbon nanofibers with high porosity: freestanding and embedded in membranes for lithium–sulfur batteries. Chem Mater 2014;26:3879–86.
[21] Sun YS, Manthiram A. A facile in situ sulfur deposition route to obtain carbon-wrapped sulfur composite cathodes for lithium–sulfur batteries. Electrochim Acta 2012;77:272–8.
[22] Werner JG, Johnson SS, Vijay V, Wiesner U. Carbon–sulfur composites from cylindrical and gyroidal mesoporous carbons with tunable properties in lithium-sulfur batteries. Chem Mater 2015;27:3349–57.
[23] Li ZJ, Lv W, Zhang C, Li BH, Kang FY, Yang QH. A sheet-like porous carbon for high-rate supercapacitors produced by the carbonization of an eggplant. Carbon 2015;92:11–4.
[24] Hu XB, Ma MH, Zeng MQ, Sun YY, Chen LF, Xue YH, et al. Supercritical carbon dioxide anchored Fe_3O_4 nanoparticles on graphene foam and lithium battery performance. ACS Appl Mater Interface 2014;6:22527–33.
[25] Deng JW, Chen LF, Sun YY, Ma MH, Fu L. Interconnected MnO_2 nanoflakes assembled on graphene foam as a binder-free and long-cycle life lithium battery anode. Carbon 2015;92:177–84.
[26] Wang J, Liu JL, Chao DL, Yan JX, Lin JY, Shen ZX. Self-assembly of honeycomb-like MoS_2 nanoarchitectures anchored into graphene foam for enhanced lithium-ion storage. Adv Mater 2014;26:7162–9.
[27] Luo JS, Liu JL, Zeng ZY, Ng CF, Ma LJ, Zhang H, et al. Three-dimensional graphene foam supported Fe_3O_4 lithium battery anodes with long cycle life and high rate capability. Nano Lett 2013;13:6136–43.
[28] Xi K, Kidambi PR, Chen RJ, Gao CL, Peng XY, Ducati C, et al. Binder free three-dimensional sulphur/few-layer graphene foam cathode with enhanced high-rate capability for rechargeable lithium sulphur batteries. Nanoscale 2014;6:5746–53.
[29] Bointon TH, Khrapach I, Yakimova R, Shytov AV, Craciun MF, Russo S. Approaching magnetic ordering in graphene materials by $FeCl_3$ intercalation. Nano Lett 2014;14:1751–5.
[30] Ferrari AC. Raman spectroscopy of graphene and graphite: disorder, electron–phonon coupling, doping and nonadiabatic effects. Solid State Commun 2007;143:47–57.
[31] Shinkarev, Fenelonov, Kuvshinov. Sulfur distribution on the surface of mesoporous nanofibrous carbon. Carbon 2003;41:295–302.
[32] Ji XL, Nazar LF. Advances in Li–S batteries. J Mater Chem 2010;20:9821–6.
[33] Wang HL, Yang Y, Liang YY, Robinson JT, Li YG, Jackson A, et al. Graphene-wrapped sulfur particles as a rechargeable lithium sulfur battery cathode material with high capacity and cycling stability. Nano Lett 2011;11:2644–7.

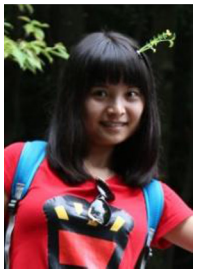

Qin Zhang is a Ph.D. student of College of Chemistry and Molecular Science, Wuhan University, Wuhan, China. After received B.S. in chemistry specialty from Huanggang Normal University in 2009, she started her Ph.D. studies at physical chemistry in Wuhan University. Her recent research focuses on the growth of graphene and its application in Li–S battery.

Prof. Lei Fu received his B.S. degree in chemistry from Wuhan University in 2001. He obtained his Ph.D. degree from the Institute of Chemistry, Chinese Academy of Sciences, in 2006. After obtaining his Ph.D., he worked as a Director's Postdoctoral Fellow at the Los Alamos National Laboratory, Los Alamos, NM (2006–2007). Thereafter, he became an associate professor of Peking University. In 2012, he joined Wuhan University as a full professor. His research interests cover two-dimensional materials and energy devices.